Journal of Biomolecular NMR, **16:** 291–302, 2000.
KLUWER/ESCOM

Transverse relaxation optimized triple-resonance NMR experiments for nucleic acids

Radovan Fiala, Jiří Czernek* & Vladimír Sklenář
Laboratory of Biomolecular Structure & Dynamics, Masaryk University, Kotlářská 2, CZ-611 37 Brno, Czech Republic; E-mail: {fiala, czernek, sklenar}@chemi.muni.cz

Received 17 December 1999; Accepted 31 January 2000

Key words: ^{13}C CSA, ^{13}C relaxation, HCN experiments, RNA, TROSY

Abstract

Triple resonance HCN and HCNCH experiments are reliable methods of establishing sugar-to-base connectivity in the NMR spectra of isotopicaly labeled oligonucleotides. However, with larger molecules the sensitivity of the experiments is drastically reduced due to relaxation processes. Since the polarization transfer between ^{13}C and ^{15}N nuclei relies on rather small heteronuclear coupling constants (11–12 Hz), the long evolution periods (up to 30–40 ms) in the pulse sequences cannot be avoided. Therefore any effort to enhance sensitivity has to concentrate on manipulating the spin system in such a way that the spin–spin relaxation rates would be minimized. In the present paper we analyze the efficiency of the two known approaches of relaxation rate control, namely the use of multiple-quantum coherence (MQ) and of the relaxation interference between chemical shift anisotropy and dipolar relaxation – TROSY. Both theoretical calculations and experimental results suggest that for the sugar moiety (H1′-C1′-N1/9) the MQ approach is clearly preferable. For the base moiety (H6/8-C6/8-N1/9), however, the TROSY shows results superior to the MQ suppression of the dipole–dipole relaxation at moderate magnetic fields (500 MHz) and the sensitivity improvement becomes dramatically more pronounced at very high fields (800 MHz). The pulse schemes of the triple-resonance HCN experiments with sensitivity optimized performance for unambiguous assignments of intra-residual sugar-to-base connectivities combining both approaches are presented.

Abbreviations: CSA, chemical shift anisotropy; MQ, multiple-quantum; SQ, single-quantum; TROSY, transverse relaxation optimized spectroscopy.

Introduction

Since the advent of techniques for the preparation of ^{13}C- and ^{15}N-labeled RNA (Batey et al., 1992; Nikonowicz et al., 1992; Michnicka et al., 1993), heteronuclear through-bond correlation experiments have become the preferable tool for resonance assignment in NMR spectra of oligonucleotides. Unlike the traditional proton-only assignment methods that rely on through-space interactions due to the nuclear Overhauser effect (NOE) (Wüthrich, 1986; Goljer and Bolton, 1994), the through-bond experiments do not depend on the spatial configuration of the studied molecule and the resulting assignment is therefore more reliable. Triple resonance HCN experiments have been proposed for sugar-to-base correlations (Farmer et al., 1993, 1994; Sklenář et al., 1993a, b; Tate et al., 1994), for sequential backbone assignments (Heus et al., 1994; Marino et al., 1994, 1995; Tate et al., 1995; Varani et al., 1995; Wijmenga et al., 1995; Ramachandran et al., 1996), and for correlating exchangeable and non-exchangeable protons in pyrimidine (Simorre et al., 1995; Sklenář et al., 1996) and purine (Fiala et al., 1996; Simorre et al., 1996a, b; Sklenář et al., 1996) bases. For optimal polarization transfer between nuclei X and Y with a coupling constant J_{XY}, an evolution delay of length $1/(2J_{XY})$

*Present address: Institute of Macromolecular Chemistry, Academy of Science of the Czech Republic, Heyrovského nám. 2, 162 06 Praha 6, Czech Republic.

is needed. Since the heteronuclear ^{13}C-^{15}N coupling constants in RNA are 12 Hz or less, a complete polarization transfer would require evolution periods of up to 100 ms long. As the spin–spin relaxation times in large RNA oligonucleotides (> 30 residues) are in the range of 20–50 ms, most of the signal is lost during the pulse sequence due to transverse relaxation. Not surprisingly, applications of the experiments mentioned above to these systems often produced disappointing results. Since different spin orders vary in their relaxation properties, keeping the spin system in the state that exhibits the slowest relaxation rate can reduce the sensitivity loss due to the relaxation processes during an experiment. Keeping a spin pair in the state of multiple-quantum coherence (MQ) eliminates most of the dipolar contribution to the spin–spin relaxation (Griffey and Redfield, 1987; Bax et al., 1989; Grzesiek and Bax, 1995). This is partially offset by a higher rate of cross-relaxation of the proton spin in the transverse plane with the remote protons as compared to the single quantum (SQ) coherence. Thanks to a rather low proton density in oligonucleotides, the use of MQ coherence proved to produce a significant sensitivity improvement in the HCN experiment (Marino et al., 1997; Fiala et al., 1998; Sklenář et al., 1998). The other approach to control the relaxation rate uses the effect of the cross-correlation between chemical shift anisotropy (CSA) and dipolar interactions (DD) which has become known as transverse relaxation optimized spectroscopy – TROSY (Pervushin et al., 1997, 1998a, b; Andersson et al., 1998; Brutscher et al., 1998; Salzmann et al., 1998, 1999; Loria et al., 1999; Rance et al., 1999). In a doublet corresponding to a J-coupled spin pair, the cross-correlated cross-relaxation between the DD and CSA mechanisms interferes constructively for one of the components (the contributions subtract) and destructively for the other (the contributions add). A refocusing pulse in the middle of an evolution interval switches the two components and eliminates the effect of the cross-correlation to the first order. If a contribution of CSA to the relaxation is significant, better sensitivity is achieved by eliminating the refocusing pulse and keeping only the slower relaxing component of the pair. The effect of cross-correlation depends on the relative size of the relaxation contribution of CSA, which in turn is a function of the magnetic field B_0. Therefore, the sensitivity increase achieved in TROSY varies with the magnetic field used. While a number of papers analyzing various aspects of the double-resonance ^{1}H-^{15}N and ^{1}H-^{13}C TROSY appeared in the literature (Pervushin et al., 1997, 1998a, b; Andersson et al., 1998; Rance et al., 1999), only one study dealing with the specifics of ^{1}H-^{13}C TROSY in nucleic acids (Brutscher et al., 1998) has been published and the three papers describing the first applications of TROSY to triple-resonance experiments (Salzmann et al., 1998, 1999; Loria et al., 1999) concentrated on proteins. In this contribution we propose experimental schemes for TROSY implementation in **H**bC**N**b *out-and-back* and **Hs**C**N**b**C**H**b** *all-the-way-through* experiments[1] for sugar-to-base correlation in labeled oligonucleotides. We provide a theoretical analysis of the relaxation processes in different versions of the experiments. Possible sensitivity gains are evaluated by theoretical simulations and experimentally demonstrated at 500 and 800 MHz on an ATP-binding aptamer complex containing 40 nucleotides.

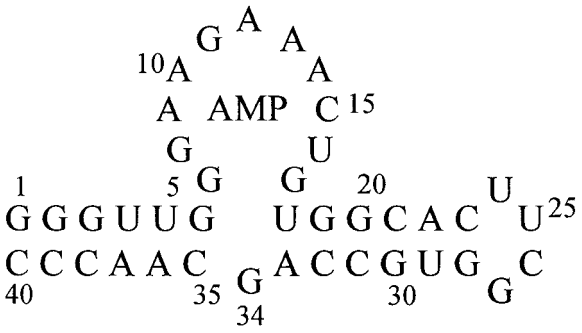

Scheme 1. The ATP-binding RNA aptamer.

Materials and methods

Sample preparation

The uniformly labeled RNA aptamer (Scheme 1) was enzymatically synthesized from labeled NTPs by in vitro transcription from a DNA template with (^{13}C, ^{15}N)-labeled nucleoside triphosphates using T7 RNA polymerase and purified by gel electrophoresis (Batey et al., 1992; Nikonowicz et al., 1993). One and a half equivalents of unlabeled AMP were added to form the complex. The final sample concentration was 3.5 mM in 99.95% D_2O with 10 mM sodium phosphate and 0.2 mM EDTA at pH 6.7. The sample was placed in a Shigemi sample tube, with a total volume of

[1]Nuclei in bold with suffix s or b denote spins on the ribose or base used for chemical shift labeling in 2D or 3D experiments, Hs/Hb indicates that correlations of both Hs and Hb are obtained at the same time.

270 μl. The details of the sample preparation have been published elsewhere (Jiang et al., 1996).

Ab initio calculations

The geometries for ab initio calculations were obtained using the following procedure.

(1) The standard geometries of adenosine, cytidine, guanidine and uridine, as implemented in the Insight/Biopolymer software package for a single-stranded A-RNA (Discover, 1996), were taken as an initial guess for full ab initio geometry optimization on the RHF/3-21G (Hehre et al., 1985) level using default options of the GAUSSIAN-94 suite of programs (Frish et al., 1995).

(2) The electron correlation effects on geometry were treated by the Density Functional Theory (DFT). The RHF/3-21G minimum served as a starting structure for optimizations using GAUSSIAN-94. The B3LYP functional (Becke, 1993) and the standard 6-31G** basis set were employed to account for the electron correlation.

We used the SOS-DFPT-IGLO methodology for the nuclear magnetic shielding tensor calculations (Malkin et al., 1995). The data in Table 1 were obtained with deMon-NMR-CS code (Malkin et al., 1994a, 1995), which implements sum-over-states density functional (Rayleigh–Schrödinger) perturbation theory with the IGLO (Kutzelnigg et al., 1990) gauge choice. The Perdew-Wang-91 exchange-correlation potential (Perdew and Wang, 1992; Perdew et al., 1997), the approximation Loc. 1 SOS-DFPT (Malkin et al., 1994a, 1995), and the basis set IGLO-III (Kutzelnigg et al., 1990) were used.

NMR spectroscopy

The NMR experiments were recorded at 298 K on Bruker Avance 500 and 800 spectrometers using triple resonance $^{1}H/^{13}C/BB$ (500 MHz) or $^{1}H/^{13}C/^{15}N$ (800 MHz) probeheads equipped with a self-shielded z-gradient coil. The spectral widths were 5 ppm in the ^{1}H dimensions and 30 ppm in the ^{15}N dimension, 512 (860 at 800 MHz) real points in t_2, 200 real points in t_1, 64 (32) scans per increment and repetition time 1.5 s. The spectra were processed using Bruker XWIN NMR software resulting in 1024 × 512 matrices; a 90°-shifted square sine-bell window function was applied in both dimensions. The schematics of the new pulse sequences for the **Hb**C**Nb**-TROSY and **Hs**C**Nb**C**Hb**-TROSY experiments are shown in Figure 1. From the sensitivity point of view, the crucial elements in the pulse sequence are the carbon-nitrogen evolution intervals. With the typical length of $\Delta = 15$ to 18 ms their contribution amounts to 60–72 ms of the length of the pulse sequence. During these intervals the C-H magnetization can be in the state of either single-quantum or multiple-quantum coherence. In the original SQ experiment (Sklenář et al., 1993b), the initial INEPT transfer produces antiphase magnetization $2H_zC_y$ that during the evolution oscillates between in-phase and antiphase magnetizations and relaxes with a corresponding relaxation rate R_2^{SQ}. In the MQ experiment, the magnetization is kept as a mixture of zero- and double-quantum coherences $2H_xC_y$ which relaxes with an average relaxation rate R_2^{MQ}. The TROSY version of the HCN experiment, while essentially similar to the SQ, allows the simultaneous use of both ^{1}H and ^{13}C steady state polarization. After the initial INEPT transfer, the magnetization can be expressed in the product operator formalism (Sörensen et al., 1983) as

$$\sigma(0) = kC_y - 2H_zC_y, \tag{1}$$

where k is the ratio of the carbon and hydrogen steady state magnetizations; for a completely relaxed system $k = \gamma_C/\gamma_H$. The relative sign of ^{13}C originating in-phase magnetization and ^{1}H originating anti-phase magnetization depends on the phase of the second proton 90° pulse and has to be chosen properly to allow the desired slow relaxing components to add. Considering the relations

$$C_y^{12} = 1/2(C_y + 2H_zC_y) \tag{2a}$$

$$C_y^{34} = 1/2(C_y - 2H_zC_y), \tag{2b}$$

we can express the magnetization of Equation 1 using the single transition operators

$$\sigma(0) = C_y^{12}(1 - k) - C_y^{34}(1 + k) \tag{3}$$

Due to the cross-correlation between the DD and CSA mechanisms the relaxation rates of the two components are different. Their respective relaxation rates can be written as

$$R_2^{12} = R_2^{DD} + R_2^{CSA} + R_2^{E} + R_2^{CC} \tag{4a}$$

$$R_2^{34} = R_2^{DD} + R_2^{CSA} + R_2^{E} - R_2^{CC} \tag{4b}$$

where the DD, CSA, E and CC superscripts denote autorelaxation from ^{13}C-^{1}H dipolar coupling of an isolated spin pair, relaxation due to ^{13}C CSA, ^{1}H cross-relaxation with neighboring protons and ^{13}C CSA and ^{13}C-^{1}H dipolar coupling cross-correlated relaxation, respectively. Note that a 180° proton pulse changes a C_y^{12} component into C_y^{34} and vice versa. It

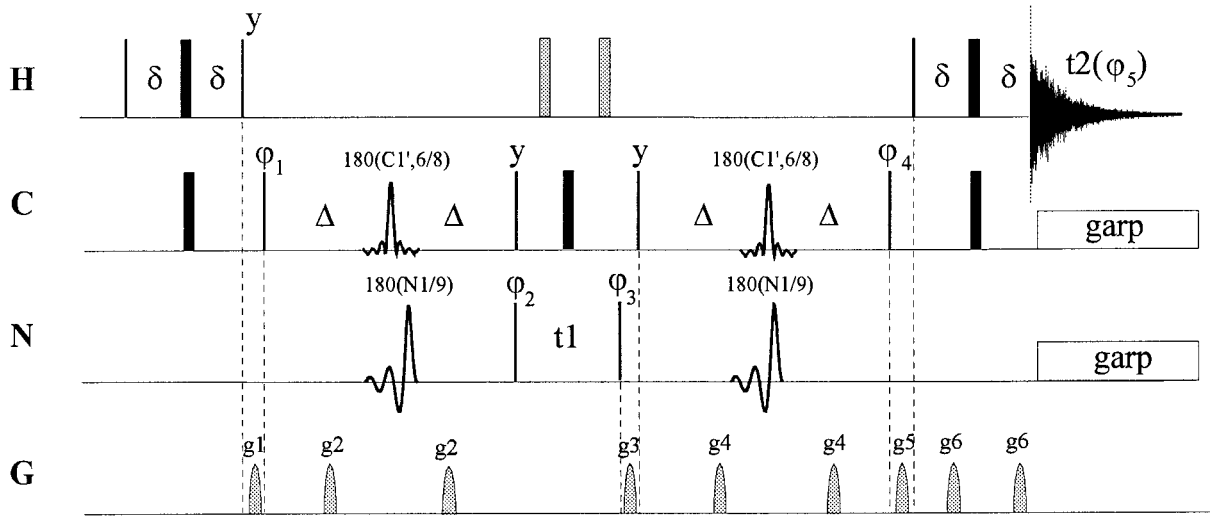

a

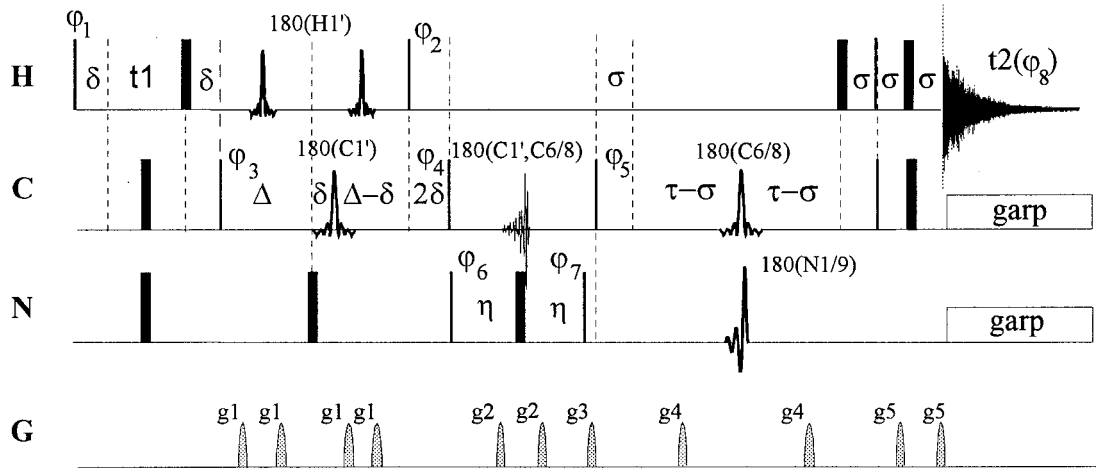

b

Figure 1. Pulse schemes for **Hb**C**Nb** *out-and-back* TROSY (Transverse Relaxation Optimized Spectroscopy) (a) and **Hs**CNC**Hb** *all-the-way-through* MQTR (multiple-quantum-TROSY) (b) experiments. The thin and thick bars represent nonselective 90° and 180° pulses, respectively; the shaded bars are optional 180° pulses. Pulses, delays and phase cycles are as follows: (a) $\delta = 1.25$ ms, $\Delta = 15$ ms. At 500 MHz the band-selective pulses were set as follows: 2.5 ms REBURP on ^{13}C centered at 140 ppm for **Hb**C**Nb** correlations; 2.0 ms IBURP-2 on ^{15}N positioned at 158 ppm. Phase cycling: φ_1 = x, −x; φ_2 = 2(x), 2(−x); φ_3 = 8(x), 8(−x); φ_4 = 4(x), 4(−x); φ_5 = abba, where a = x, −x, −x, x, and b = −x, x, x, −x. In addition, φ_3 is incremented in the States-TPPI manner to achieve quadrature detection in the F_1 dimension. (b) $\delta = 1.6$ ms, $\Delta = 15.0$ ms, $\eta = 18.0$ ms, $\tau = 15.0$ ms, $\sigma = 1.25$ ms. At 500 MHz the band-selective pulses were set as follows: 180(C1′): 2.862 ms REBURP centered at 90 ppm, 180(C1′, C6/8): 3.0 ms IBURP2 pulse with additional cosine modulation (f_m = 3144 Hz) to provide inversion at 90±4.3 and 140±4.3 ppm, 180(C6/8): 2.862 ms REBURP centered at 140 ppm, 180(N1/9): 2.0 ms IBURP-2 pulse centered at 158 ppm, 180(H1′): 4.0 ms REBURP centered at 5.7 ppm. Phase cycling: φ_1 = x + States-TPPI; φ_2 = 4(y), 4(−y); φ_3 = 2(x), 2(−x); φ_4 = 16(x), 16(−x); φ_5 = x, −x; φ_6 = 32(x), 32(−x); φ_7 = 8(x), 8(−x); φ_8 = abba, 2(baab), abba, where a = x, −x, −x, x, and b = −x, x, x, −x. The same gradient pulses as in Figure 1a were used. For a 3D version of the experiment, **Hs**C**Nb**C**Hb**, the phase φ_6 can be incremented for the States-TPPI quadrature detection in the ^{15}N dimension and the delay η can be varied in a constant time manner. The pulses were applied along the x-axis unless otherwise specified. At 800 MHz, all the band-selective pulses were set to 62.5% of their durations specified above. Sine-bell modulated gradient pulses of 800 μs duration were applied with the strengths g1 = 4.2, g2 = 2.5, g3 = 4.8, g4 = 7.2, g5 = 9.0, g6 = 8.4 G/cm followed by 100 μs recovery delays. GARP decoupling (Shaka et al., 1985) of ^{13}C and ^{15}N was used during detection.

Table 1. CSA parameters calculated ab initio for selected carbon and hydrogen atoms in RNA nucleosides

	σ_{11} (ppm)	σ_{22} (ppm)	σ_{33} (ppm)	θ_x (°)	θ_y (°)	θ_z (°)	δ (ppm)	$\Delta\sigma$ (ppm)	Γ (ppm)
C8(G)	−27.4	55.5	109.0	30.4	120.4	89.1	138.2	119.0	−77.8
C8(A)	−29.5	46.4	112.2	29.4	119.4	89.8	140.8	122.8	−81.4
C6(C)	−60.7	23.5	150.2	26.9	117.9	89.3	146.2	183.9	−121.6
C6(U)	−64.3	39.5	148.3	25.7	115.7	89.5	142.7	184.1	−128.9
C1′(G)	64.0	80.5	111.2	22.7	109.1	78.2	98.6	41.5	−25.2
C1′(A)	64.2	79.9	110.4	21.5	107.7	78.2	99.0	40.7	−25.9
C1′(C)	63.4	78.8	106.1	28.6	116.2	79.3	101.1	37.4	−22.3
C1′(U)	63.9	79.3	108.0	23.5	111.5	81.0	100.2	38.8	−25.0
H8(G)	15.5	24.3	28.4	90.0	136.6	46.6	8.6	11.4	−3.9
H8(A)	14.8	23.8	28.5	87.9	137.7	47.8	8.9	12.1	−3.9
H6(C)	16.7	21.8	29.2	77.3	144.2	57.2	8.7	10.8	−2.8
H6(U)	16.7	22.1	29.0	78.7	144.9	57.2	8.7	10.6	−2.7
H1′(G)	19.9	24.6	30.2	78.2	126.6	39.1	6.4	8.9	−4.3
H1′(A)	19.6	24.8	29.5	77.7	121.1	33.9	6.6	8.6	−4.8
H1′(C)	21.8	24.7	29.3	88.4	121.5	31.5	6.0	6.6	−4.0
H1′(U)	21.5	24.6	29.3	85.3	125.2	35.6	6.1	6.9	−3.9

σ_{11}, σ_{22} and σ_{33} are the principal component of the chemical shielding tensor, θ_x, θ_y and θ_z are the angles between the corresponding tensor component and the C-H bond, δ is the (TMS referenced) isotropic chemical shift calculated as $\delta = \sigma_{TMS} - (\sigma_{11} + \sigma_{22} + \sigma_{33})/3$, where σ_{TMS} values were 183.87 and 31.27 ppm for C and H, respectively, $\Delta\sigma$ is CSA and Δ_{CC} is the part of CSA responsible for cross relaxation calculated from the shielding tensor components according to the relations (Brutscher et al., 1998): $\Delta\sigma = \sqrt{(\sigma_x^2 + \sigma_y^2 - \sigma_x\sigma_y)}$, $\Gamma = \sigma_x P_2(\cos\theta_x) + \sigma_y P_2(\cos\theta_y)$, $\sigma_x = \sigma_{33} - \sigma_{11}$, $\sigma_y = \sigma_{33} - \sigma_{22}$, $P_2(x)$ is the second-rank Legendre polynomial.

follows that, to achieve the advantage of the reduced relaxation rate, no proton refocusing pulses are allowed between the initial and the final INEPT steps. This condition is not met in the SQ experiment because of the ^{1}H 180° pulse in the middle of the t_1 period. At this point, the fast and the slow relaxing component are switched for the second C-N evolution period, resulting in the averaged relaxation rate R_2. If the $^2J_{HN}$ coupling caused a loss of sensitivity loss due to the line broadening in the ^{15}N dimension, the interaction can be decoupled in TROSY by applying two proton refocusing pulses instead of one, placed at $t_1/4$ and $3t_1/4$ points. In this case, the two components are switched only for a period of $t_1/2$, which is much shorter than 2Δ and does not result in significant sensitivity loss. With the 2D or 3D **Hs**C**Nb**C**Hb** experiment there are some important differences. First, since the 2D experiment is ^{1}H-^{1}H correlation and the 3D version correlates ^{1}H-^{15}N-^{1}H, it is in principle impossible to combine the contribution from ^{1}H and ^{13}C steady state magnetizations. Second, the SQ pulse sequence does not have a proton refocusing pulse in the center and, unlike in the **Hs**/**Hb**C**Nb** *out-and-back* experiment, the relaxation rates of the two components in the CH doublet are not averaged. This means that the original SQ **Hs**CNC**Hb** pulse sequence (Sklenář et al., 1993a) accidentally involves the principle more recently utilized in the TROSY experiments. This explains why the sensitivity increase of the MQ over the SQ version of the **Hb**CNC**Hb** experiment is substantially lower than the corresponding increase in the **Hb**C**Nb** experiment (Fiala et al., 1998). The ^{1}H 180° pulse in the C-N evolution period does have the effect of interchanging C_y^{12} and C_y^{34} components. This pulse is necessary to provide ^{13}C magnetization in-phase with respect to its attached ^{1}H before the transfer to ^{15}N and cannot therefore be omitted. However, the pulse is placed asymmetrically in the C-N evolution period and an arrangement is possible where the magnetization relaxes with the faster relaxation rate R_2^{12} for the short interval δ and with the slow rate R_2^{34} for the rest of the period, i.e. 2Δ–δ. With δ set optimally at $1/(4J_{HC})$ and a typical value for the aromatic moiety H6/8-C6/8 of $\delta = 1.25$ ms, much of the TROSY sensitivity increase is retained. As we will discuss

later, the values of CSA for the C1′ carbon are low and therefore the cross-correlation effect here is insignificant. The optimized pulse sequence (Figure 1b) therefore uses the MQ magnetization in the transfer from the H1′→C1′→N1/9 and the TROSY method (identical with SQ here) for the magnetization transfer N1/9→C6/8→H6/8. The pulse sequences described here use broadband decoupling during acquisition since the CSA values of both sugar and base protons are too small (see Table 1) to provide any significant TROSY effect.

Relaxation rate simulations

The relaxation rate constants for ^{13}C SQ and ^{1}H-^{13}C MQ coherences and the slowly relaxing component of the doublet were calculated according to the following equations (Goldman, 1984; Peng and Wagner, 1994; Fushman and Cowburn, 1999; Rance et al., 1999):

$$\begin{aligned} R_2^{SQ} &= d_{CH}^2/8[4J(0) + J(\omega_H - \omega_C) + 3J(\omega_C) \\ &\quad +3J(\omega_H) + 6J(\omega_H + \omega_C)] \\ &\quad +(c_C^2/6)[4J(0) + 3J(2\omega_C)] \\ &\quad +(c_H^2/2)J(\omega_H) + \sum d_{HH}^2/8[J(0) \\ &\quad +3J(\omega_H) + 6J(2\omega_H)] \end{aligned} \tag{5}$$

$$\begin{aligned} R_2^{MQ} &= d_{CH}^2/8[J(\omega_H - \omega_C) \\ &\quad +3J(\omega_C) + 3J(\omega_H) + 6J(\omega_H + \omega_C)] \\ &\quad +(c_C^2/6)[4J(0) + 3J(\omega_C)] \\ &\quad +(c_H^2/6)[4J(0) + 3J(\omega_H)] \\ &\quad + \sum d_{HH}^2/8[5J(0) + 9J(\omega_H) \\ &\quad +6J(2\omega_H)] \end{aligned} \tag{6}$$

$$\begin{aligned} R_2^{TR} &= d_{CH}^2/8[4J(0) + J(\omega_H - \omega_C) \\ &\quad +3J(\omega_C) + 3J(\omega_H) + 6J(\omega_H + \omega_C)] \\ &\quad +(c_C^2/6)[4J(0) + 3J(\omega_C)] + (c_H^2/2) \\ &\quad 3J(\omega_H) + 1/(2\sqrt{3})g_C d_{HC}[4J(0) \\ &\quad +3J(\omega_C)] + \sum d_{HH}^2/8[J(0) + 3J(\omega_H) \\ &\quad +6J(2\omega_H)] \end{aligned} \tag{7}$$

where

$$d_{XY} = \gamma_X \gamma_Y h\mu_0/(8\pi^2 r_{XY}^3) \tag{8}$$

$$c_X = \omega_X \Delta\sigma_X/\sqrt{3} \tag{9a}$$

$$g_X = \omega_X \Gamma_X/\sqrt{3} \tag{9b}$$

μ_0 is the permittivity of free space, h is Planck's constant, γ_X is the gyromagnetic ratio of the spin X, r_{XY} is the distance of the nuclei X and Y, ω_X is the Larmor frequency of spin X and $\Delta\sigma_X$ and Γ_X are the chemical shift anisotropies of X defined as indicated in the footnotes to Table 1. The spectral density function was assumed in the form (Cavanagh et al., 1996)

$$\begin{aligned} J(\omega) &= 2/5[S^2\tau_m/(1 + \omega^2\tau_m^2) \\ &\quad +(1 - S^2)\tau/(1 + \omega^2\tau^2)] \end{aligned} \tag{10}$$

The rotation correlation times were estimated for the studied molecule at 298 K as $\tau_m = 8.10^{-9}$ and $\tau = 8.10^{-12}$ s. The calculations were performed for the case of a rigid molecule ($S^2 = 1.0$) and a moderately flexible molecule ($S^2 = 0.75$).

Results and discussion

Chemical shift anisotropy

The ab initio calculations have been performed for both RHF and B3LYP geometries. The geometry strongly affected ^{1}H shielding tensors. The shielding of the hydrogen nuclei was too high when RHF/3-21G geometry was employed, mainly due to considerably shorter C–H bond lengths obtained on this level. We have observed discrepancies in the orientation of the principal components of some ^{1}H shielding tensors as well (data not shown). On the other hand, ^{13}C tensors remain essentially unaffected by the geometry. The results reported in Table 1 are for the B3LYP/6-31G** optimized structures only. The bond lengths at the B3LYP global minimum of adenine are very close to the values found using neutron diffraction (Klooster et al., 1991) at 123 K (e.g., for the bond length C8–H8 a value of 1.080 Å has been reported). Therefore, we consider the geometries used reliable for the purpose of our study. The discrepancies between experimental chemical shifts and values from Table 1 can be attributed mainly to neglect of the site-specific interactions present in the investigated aptamer. Computed values of the tensor components, $\Delta\sigma$, and θ are in reasonable agreement with the data published for the simplified models of nucleosides by Case and coworkers (Dejaegere and Case, 1998; Sitkoff and Case, 1998).

As expected, the $\Delta\sigma$ values of C1′ atoms are much smaller than in the case of C6/8. However, there is also an important difference in the values of $\Delta\sigma$ between purine and pyrimidine nucleosides. Namely, the values of $\Delta\sigma$ are substantially ($\sim$ 60 ppm) larger for the latter. Simultaneously, the angles θ_x are slightly larger in purines, thus further increasing the difference

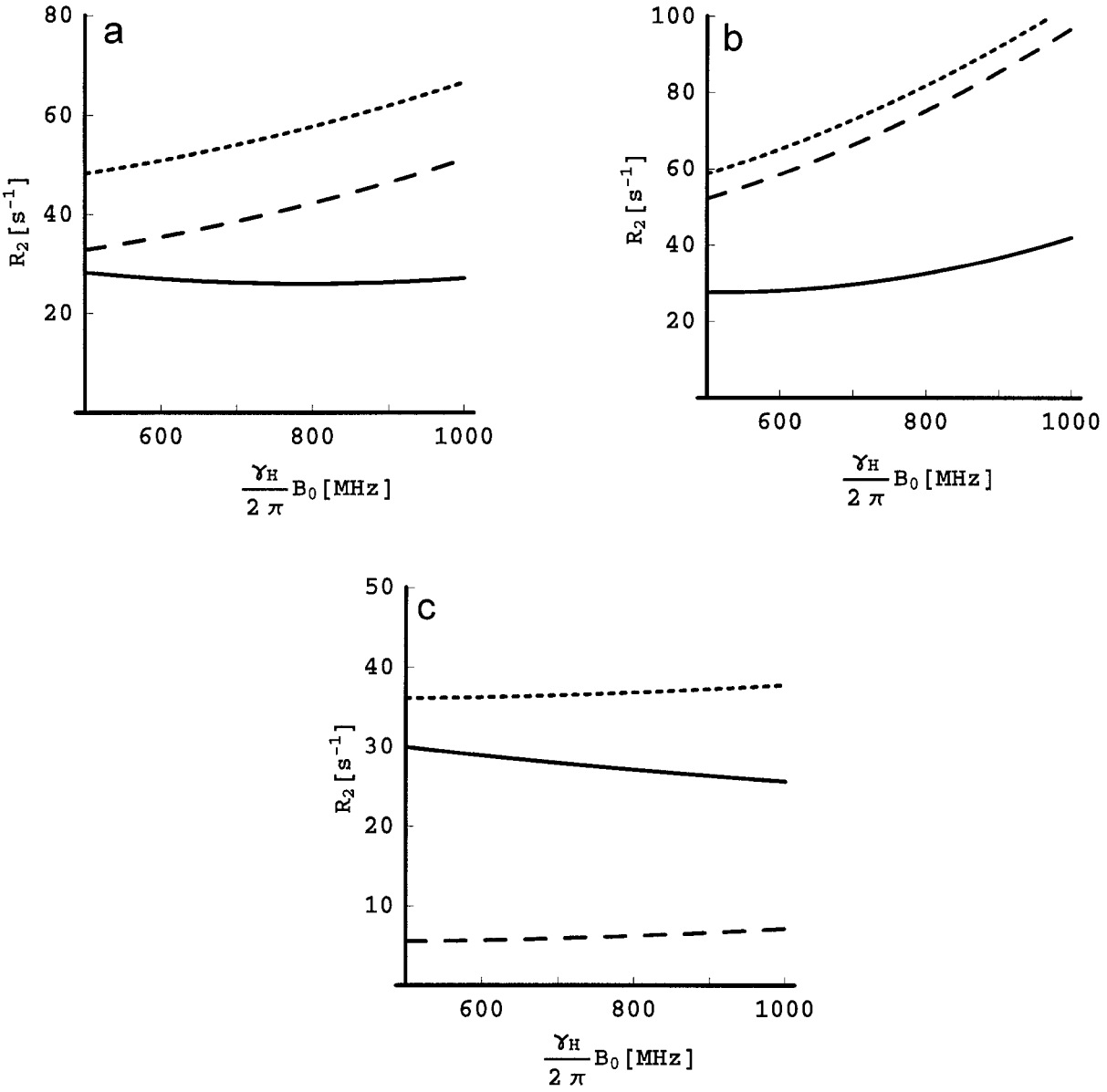

Figure 2. The transverse relaxation rate dependence on the static magnetic field B_0 calculated for (a) C8 of guanine, (b) C6 of cytosine and (c) C1′ (average value for all nucleosides). Short dashes: single-quantum coherence; long dashes: multiple-quantum coherence; solid line: the slowly relaxing (TROSY) component of the CH doublet.

in the effect of cross-correlation. For all carbon nuclei the orientation of the shielding components is rather uniform with $\sigma_{\|}$ close to the σ_{11} principal element. In the case of H6/8 and H1′, the components closest to the C–H bond vector are σ_{33}. For the ^{1}H shielding tensors the difference between bases and corresponding nucleosides is significant. On the other hand, the presence of the (deoxy)ribose ring only moderately affects the C6/8 shielding.

Relaxation rates

The relaxation rates for SQ, MQ and TR magnetizations were calculated according to Equations 5–7 and the results are summarized in Table 2. We also studied the effect on the relaxation rates of distant protons and intramolecular motions. The relaxation contributions due to the dipolar effect of the adjacent heteroatoms is small enough to be neglected, less than 2% of the contribution from the directly attached proton for car-

Table 2. Spin–spin relaxation rates for single quantum coherence, multiple quantum coherence and the slowly relaxing component of the doublet for selected carbon atoms in RNA nucleosides at 11.75 and 18.8 T

	500 MHz			800 MHz		
	$R_{2,SQ}$ (s^{-1})	$R_{2,MQ}$ (s^{-1})	$R_{2,TR}$ (s^{-1})	$R_{2,SQ}$ (s^{-1})	$R_{2,MQ}$ (s^{-1})	$R_{2,TR}$ (s^{-1})
C6(C)[a]	51.6	16.9	20.5	74.6	41.2	25.3
C8(G)[a]	43.3	8.1	23.2	52.6	18.9	20.9
C8(A)[a]	43.7	8.6	22.7	53.7	20.2	20.5
C6(U)[a]	52.2	16.9	19.0	75.3	41.2	22.6
C1′[a,e]	37.6	2.0	30.1	38.2	3.5	26.4
C6(C)[b]	38.7	12.7	15.4	56.0	30.9	19.0
C8(G)[b]	32.5	6.1	17.5	39.5	14.2	15.7
C8(A)[b]	32.8	6.5	17.1	40.3	15.2	15.4
C6(U)[b]	39.2	12.7	14.3	56.5	30.9	17.0
C1′[b,e]	28.2	1.6	22.6	28.7	2.6	19.8
C6(C)[c]	58.9	53.4	27.8	81.9	77.6	32.6
C8(G)[c]	48.4	33.7	28.4	57.8	44.4	26.0
C8(A)[c]	48.8	34.2	27.8	58.8	45.7	25.6
C6(U)[c]	59.6	53.4	26.3	82.6	77.6	29.9
C1′[c,e]	38.4	6.2	31.0	39.0	7.7	27.2
C6(C)[d]	51.9	47.1	22.7	71.9	68.1	25.7
C8(G)[d]	42.7	29.8	25.8	50.7	39.0	24.1
C8(A)[d]	43.1	30.3	24.9	51.6	40.2	22.9
C6(U)[d]	52.5	47.1	22.9	72.5	68.1	25.9
C1′[d,e]	33.9	5.7	27.3	34.3	6.8	23.9

[a]Isolated rigid spin pair.
[b]Isolated pair and dynamics characterized by an order parameter of $S^2 = 0.75$.
[c]Rigid C-H pair with remote protons included[f].
[d]C-H pair with remote protons and dynamics ($S^2 = 0.75$) taken into account.
[e]Sugar C1′ values are averages for all nucleosides.
[f]Remote proton distances: H6 at 3.2, 2.2, 2.4, 2.0, and 3.0 Å for intraresidual H2′, H3′ and H5 and sequential H2′ and H3′, respectively. H8 at 3.3, 2.2, 2.1, and 3.0 Å for intraresidual H2′ and H3′ and sequential H2′ and H3′, respectively. H1′ at 2.7, 3.4, and 3.6 Å for intraresidual H2′, H4′ and sequential H2.

bon and even less for nitrogen atoms. In all cases, the effect of the distribution of other ^{1}H nuclei in the vicinity of the studied C-H spin pair is significant. This is especially true for MQ coherence, where we found differences up to several hundred per cent within the family of structures deposited in the Brookhaven database for the studied aptamer. This prevented us from calculating the relaxation rates for specific residues in the molecule with any reasonable degree of accuracy. On the other hand, this high structural sensitivity of the MQ relaxation rates in principle opens a possibility for exploiting the relaxation rate information in structure determination studies. A crucial parameter for the efficiency of the TROSY approach is the static magnetic field B_0. Figure 2 shows the dependence of R_2^{SQ}, R_2^{MQ} and R_2^{TR} on B_0 for guanine C8, cytosine C6 and (average) sugar C1′. For higher values of CSA, the optimum TROSY relaxation is achieved at lower fields and the relaxation rate reduction is more pronounced. The non-colinearity of the carbon CSA with the C-H bond causes that the minimum on the R_2^{TR} curve appears at lower B_0, but it is shallower, i.e. the relaxation rate reduction is less effective. For the individual bases we found optima at 18.3, 18.6, 12.2, and 12.9 T for adenine, guanine, cytosine, and uracil, respectively. For sugar C1′ the optimum lies at over 50 T, far beyond the currently available magnetic fields. We can see that for the pyrimidines, the optimal TROSY performance occurs at fields between 500 and 600 MHz while for the purines the optimum is achieved at a much higher field of about 780 MHz. The minimum is quite broad in both cases, however. Moreover, SQ and MQ relaxation rates grow rather quickly with the increasing magnetic field due to large values of base carbon CSAs. As a result, the sensitivity increase of the TROSY experiment over both SQ

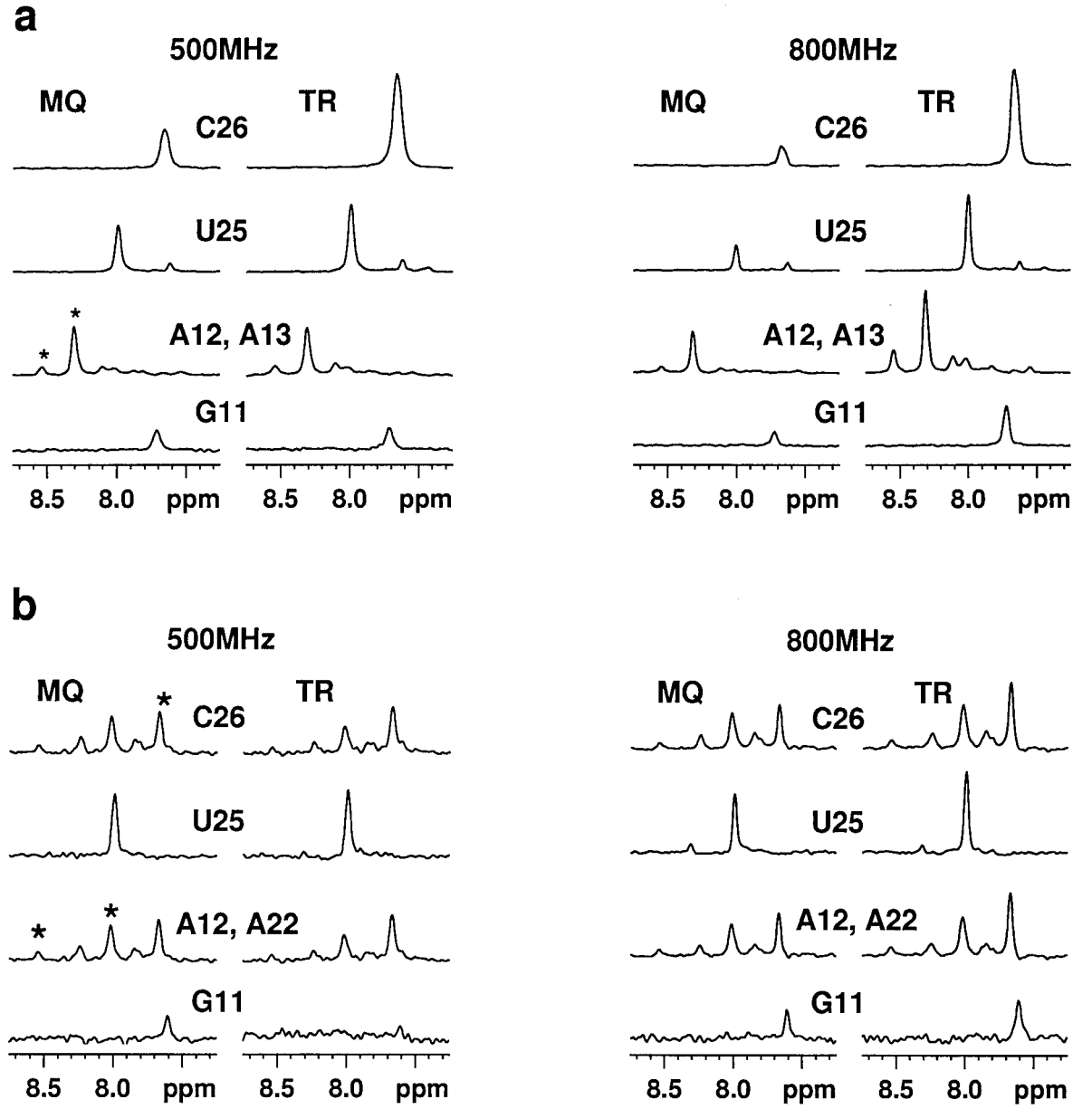

Figure 3. Traces from 2D (a) **HbCNb** and (b) **Hs**CNC**Hb** spectra illustrating the sensitivity differences of MQ and TROSY versions of the experiments at 500 and 800 MHz for the residues indicated in the figures. The relevant peaks are labeled with asterisks where necessary. The plot scales may vary between different residues.

and MQ is significantly higher at 800 MHz than at 500 MHz.

Sensitivity

We chose to compare the TROSY experiments with the most sensitive existing versions, namely the selective MQ experiments that showed superior sensitivity in the previous studies (Fiala et al., 1998). Since the low values of CSA for the sugar C1′ carbon do not offer suitable conditions for TROSY we applied the method to the base correlations only. The MQ and TROSY experiments differ only in the relaxation rates during the evolution of the CN magnetization. The expected effect of the relaxation on the signal intensity during this period can be calculated for multiple-quantum coherence as

Table 3. Calculated and experimental sensitivity gain[a] $G = I_{TR}/I_{MQ}$ of the TROSY over the MQ version of the **H**C**N** and **H**CNC**H** experiments at 11.75 and 18.8 T

	500 MHz			800 MHz		
	G_{calc}[b]	G_{calc}[c]	G_{exp}	G_{calc}[b]	G_{calc}[c]	G_{exp}
HC**N**						
C6	3.48	3.24	2.81	11.13	9.55	9.79
G8	1.03	0.95	1.05	2.26	1.83	2.96
A8	1.10	1.04	0.94	2.51	2.12	3.07
U6	3.81	3.20	3.07	13.10	9.43	7.44
C1′[d]	0.17	0.21	–	0.23	0.27	–
HCNC**H**						
C6	1.00	0.97	1.00	1.70	1.59	1.71
G8	0.56	0.54	0.76	0.80	0.73	1.13
A8	0.57	0.56	0.76	0.84	0.78	1.31
U6	1.04	0.96	1.06	1.83	1.58	1.55
C1′[d]	0.23	0.26	–	0.27	0.29	–

[a]For the purpose of the calculations, INEPT transfer was considered 100% efficient.
[b]Rigid ($S^2 = 1$) site.
[c]Flexible ($S^2 = 0.75$) site. In both cases, remote protons were taken into account.
[d]Average values for all nucleosides.

$$I^{MQ} = I_0 \exp(-R_2^{MQ} T_t) \tag{11}$$

and for TROSY

$$I^{TR} = 1/2 I_0 (m + k) \exp(-R_2^{TR} T_t). \tag{12}$$

Equation 12 considers the fact that only one component of the doublet relaxes slowly. The coefficients $m \leq 1$ and $k \geq \gamma_C/\gamma_H$ account for the limited efficiency of the INEPT transfer and for the contribution of the ^{13}C steady-state magnetization, respectively. The total time T_t during the applicable evolution periods was $T_t = 4\Delta = 60$ ms in the 2D **Hs**/**Hb**C**Nb** experiment and $T_t = 2\tau - \sigma = 28.75$ ms in the 2D **Hs**CNC**Hb** experiment. A comparison of experimental sensitivity gains and corresponding values expected based on calculated relaxation rates for MQ and TR is given in Table 3 and examples of experimental peak amplitudes are shown in Figure 3. The experimental data generally confirm well the theoretical predictions. However, for several reasons it is impossible to reproduce experimental data exactly. As we mentioned above, the MQ relaxation rates are extremely sensitive to the proton environment of the C-H moiety as well as to the site mobility. Therefore, the precision with which the structure is known has a considerable influence on variations in the calculated relaxation times. For the calculations, we used generic interproton distances (Wüthrich, 1986; Goljer and Bolton, 1994) for A-type RNA and the experimental data are averages over four nucleotides of each type in the molecule. The simulated data in Table 3 seems to understate systematically the TROSY sensitivity with purines and overstate it with pyrimidines. We should note here that due to the high sensitivity of R_2^{MQ} to distant protons, a minor change of about 0.2 Å in the interproton distance to the closest neighbor would reverse the trend. In some cases, the experimental amplitudes cannot be reliably evaluated due to peak overlap or because the amplitudes of the MQ peak are imprecise due to a very low signal/noise ratio. The contribution of the ^{13}C steady-state magnetization depends on the ratio of ^1H and ^{13}C spin-lattice relaxation times and the value of k is typically greater than 0.25. Brutscher et al. (1998) reported values of $1 + k$ in the range 1.5–2.0 for a partially labelled RNA 33-mer and repetition times of 1.5 s. The data in Table 3 were calculated using a value of $k = 0.5$. Finally, the relaxation rates are affected by intramolecular dynamics of the studied molecule, of which nothing is known yet. From the data shown it is evident that the **Hs**/**Hb**C**Nb**-TROSY experiment is superior to the other versions for base proton to glycosidic nitrogen correlation. With the **Hs**CNbC**Hb** experiments, the situation is less favorable, as reduced R_2 in TROSY can only be used in one half of the pulse sequence. Also, the benefit of the ^{13}C steady-state magnetization is not available in the ^1H-^1H correlation experiment. Significant sensitivity enhancement can be achieved only in pyrimidines and mainly at the highest magnetic fields (750–800 MHz).

Conclusions

Theoretical analysis, based on ab initio calculated carbon CSA, suggests that significant sensitivity improvement can be achieved in triple-resonance NMR experiments with the use of the slowly relaxing magnetization component of the base carbon nuclei. The approach is more efficient with pyrimidines than with purines due to the larger values of pyrimidine C6 CSA. The sensitivity gain is strongly field dependent and becomes quite dramatic for the highest magnetic fields. With the **Hb**C**Nb**-TROSY experiment at 800 MHz, we found sensitivity enhancements over the best existing experiment by a factor of ∼3 for purines and in the range of 5–10 for pyrimidines in the case of H6/8-N1/9 correlation. For the H1′-N1/9 correlation, the low value of C1′ CSA does not allow for efficient application of the TROSY principle, leaving the

selective multiple-quantum **Hs**C**Ns** experiment (Fiala et al., 1998) as the most sensitive approach. The **Hs**CNbC**Hb** correlation experiments do not allow the full use of the benefits of the TROSY approach. In spite of that, significant sensitivity improvements, by a factor of 1.1–1.7, can be achieved at 800 MHz.

Acknowledgements

The research has been supported by the Grant Agency of the Czech Republic, Grant No. 203/99/0311. We thank Dr. Dinshaw Patel and Feng J. Sam of the Memorial Sloan-Kettering Cancer Center for the sample of ATP-binding RNA aptamer used in this study and Dr. Wolfgang Bermel and Bruker Analytik GmbH for providing experimental time on the 800 MHz spectrometer.

References

Andersson, P., Annila, A. and Otting, G. (1998) *J. Magn. Reson.*, **133**, 364–367.

Batey, R.T., Inada, M., Kujawinski, E., Puglisi, J.D. and Williamson, J.R. (1992) *Nucleic Acids Res.*, **20**, 4515–4523.

Bax, A., Kay, L.E., Sparks, S.W. and Torchia, D.A. (1989) *J. Am. Chem. Soc.*, **111**, 408–409.

Becke, A.D. (1993) *J. Chem. Phys.*, **98**, 5648–5652.

Brutscher, B., Boisbouvier, J., Pardi, A., Marion, D. and Simorre, J.-P. (1998) *J. Am. Chem. Soc.*, **120**, 11845–11851.

Cavanagh, J., Fairbrother, W.J., Palmer, A.G. and Skelton, N.J. (1996) *Protein NMR Spectroscopy: Principles and Practice*, Academic Press, San Diego, CA, p. 269.

Dejaegere, A. and Case, D.A. (1998) *J. Phys. Chem.*, **A102**, 5280–5289.

Discover 96.0 (1996) *User Guide*, version 4.0.0, Molecular Simulations, San Diego, CA.

Farmer, B.T., Müller, L., Nikonowicz, E.P. and Pardi, A. (1993) *J. Am. Chem. Soc.*, **115**, 11040–11041.

Farmer, B.T., Müller, L., Nikonowicz, E.P. and Pardi, A. (1994) *J. Biomol. NMR*, **4**, 129–133.

Fiala, R., Jiang, F. and Patel, D.J. (1996) *J. Am. Chem. Soc.*, **118**, 689–690.

Fiala, R., Jiang, F. and Sklenář, V. (1998) *J. Biomol. NMR*, **12**, 373–383.

Fiolhais, C. (1992) *Phys. Rev.*, **B46**, 6671–6687.

Frish, M.J., Trucks, G.W., Schlegel, H.B., Gill, P.M.W., Johnson, B.G., Robb, M.A., Cheeseman, J.R., Keith, T., Petersson, G.A., Montgomery, J.A., Raghavachari, K., Al-Laham, M.A., Zakrzewski, V.G., Ortiz, J.V., Foresman, J.B., Cioslowski, J., Stefanov, B.B., Nanayakkara, A., Challacombe, M., Peng, C.Y., Ayala, P.Y., Chen, W., Wong, N.M., Andres, J.L., Replongle, E.S., Gomperts, R., Martin, R.L., Fox, D.J., Binkley, J.S., Defrees, D.J., Baker, J., Stewart, J.P., Head-Gordon, M., Gonzales, C. and Pople, J.A. (1995) *Gaussian 94 Revision C.2*, Gaussian, Inc., Pittsburgh, PA.

Fushman, D. and Cowburn, D. (1999) *J. Biomol. NMR*, **13**, 139–147.

Goldman, M. (1984) *J. Magn. Reson.*, **60**, 437–452.

Goljer, I. and Bolton, P.H. (1994) In *Two-Dimensional Spectroscopy. Applications for Chemists and Biochemists* (Eds, Croasmun, W.R. and Carlson, R.M.K.), VCH Publishers, New York, NY, pp. 699–740.

Griffey, R.H. and Redfield, A.G. (1987) *Q. Rev. Biophys.*, **19**, 51–82.

Grzesiek, S. and Bax, A. (1995) *J. Biomol. NMR*, **6**, 335–339.

Hehre, W.J., Radom, L., Schleyer, P.v.R. and Pople, J.A. (1985) *Ab initio Molecular Orbital Theory*, Wiley-Interscience, New York, NY.

Heus, H.A., Wijmenga, S.S., van de Ven, F.J.M. and Hilbers, C.W. (1994) *J. Am. Chem. Soc.*, **116**, 4983–4984.

Jiang, F., Fiala, R., Live, D., Kumar, R.A. and Patel, D.J. (1996) *Biochemistry*, **35**, 13250–13266.

Klooster, W.T., Ruble, J.R. and Craven, B.M. (1991) *Acta Crystallogr.*, **B47**, 376–383.

Kutzelnigg, W., Fleisher, U. and Schindler, M. (1990) *NMR Basic Principles and Progress*, Vol. 23, Springer-Verlag, Berlin, Heidelberg, pp. 167–262.

Loria, J.P., Rance, M. and Palmer III, A.G. (1999) *J. Magn. Reson.*, **141**, 180–184.

Malkin, V.G., Malkina, O.L., Casida, M.E. and Salahub, D.R. (1994a) *J. Am. Chem. Soc.*, **116**, 5898–5908.

Malkin, V.G., Malkina, O.L. and Salahub, D.R. (1994b) *MASTER-CS Program*, Université de Montreal, Montreal, Canada.

Malkin, V.G., Malkina, O.L., Eriksson, L.A. and Salahub, D.R. (1995) In *Theoretical and Computational Chemistry*, Vol. 2 (Eds, Seminario, J.M. and Politzer, P.), Elsevier, Amsterdam, pp. 273–401.

Marino, J.P., Diener, J.L., Moore, P.B. and Griesinger, C. (1987) *J. Am. Chem. Soc.*, **119**, 7361–7366.

Marino, J.P., Schwalbe, H., Anklin, C., Bermel, W., Crothers, D.M. and Griesinger, C. (1995) *J. Biomol. NMR*, **5**, 87–92.

Michnicka, M.J., Harper, J.W. and King, G.C. (1993) *Biochemistry*, **32**, 395–400.

Nikonowicz, E.P., Sirr, A., Legault, P., Jucker, F.M., Baer, L.M. and Pardi, A. (1992) *Nucleic Acids Res.*, **20**, 4507–4513.

Peng, J.W. and Wagner, G. (1994) *Methods Enzymol.*, **239**, 563–596.

Perdew, J.P. and Wang, Y. (1992) *Phys. Rev.*, **B45**, 13244–13249.

Perdew, J.P., Chevary, J.A., Vosko, S.H., Jackson, K.A., Pederson, M.R., Singh, D.J., Pervushin, K., Riek, R., Wider, G. and Wüthrich, K. (1997) *Proc. Natl. Acad. Sci. USA*, **94**, 12366–12371.

Pervushin, K., Ono, A., Fernández, C., Szyperski, T., Kainosho, M. and Wüthrich, K. (1998a) *Proc. Natl. Acad. Sci. USA*, **95**, 14147–14151.

Pervushin, K., Riek, R., Wider, G. and Wüthrich, K. (1998b) *J. Am. Chem. Soc.*, **120**, 6394–6400.

Pervushin, K., Wider, G. and Wüthrich, K. (1998c) *J. Biomol. NMR*, **12**, 345–348.

Ramachandran, R., Sich, C., Grüne, M., Soskic, V. and Brown, L.R. (1996) *J. Biomol. NMR*, **7**, 251–255.

Rance, M., Loria, J.P. and Palmer, A.G. (1999) *J. Magn. Reson.*, **136**, 92–101.

Salzmann, M., Pervushin, K., Wider, G., Senn, H. and Wüthrich, K. (1998) *Proc. Natl. Acad. Sci. USA*, **95**, 13585–13590.

Salzmann, M., Wider, G., Pervushin, K., Senn, H. and Wüthrich, K. (1999) *J. Am. Chem. Soc.*, **121**, 844–848.

Shaka, A.J., Barker, P. and Freeman, R. (1985) *J. Magn. Reson.*, **64**, 547–552.

Simorre, J.-P., Zimmermann, G.R., Pardi, A., Farmer II, B.T. and Mueller, L. (1995) *J. Biomol. NMR*, **6**, 427–432.

Simorre, J.-P., Zimmermann, G.R., Mueller, L. and Pardi, A. (1996a) *J. Biomol. NMR*, **7**, 153–156.
Simorre, J.-P., Zimmermann, G.R., Mueller, L. and Pardi, A. (1996b) *J. Am. Chem. Soc.*, **118**, 5316–5317.
Sitkoff, D. and Case, D.A. (1998) *Prog. NMR Spectrosc.*, **32**, 165 – 229.
Sklenář, V., Peterson, R.D., Rejante, M.R., Wang, E. and Feigon, J. (1993a) *J. Am. Chem. Soc.*, **115**, 12181–12182.
Sklenář, V., Peterson, R.D., Rejante, M.R. and Feigon, J. (1993b) *J. Biomol. NMR*, **3**, 721–727.
Sklenář, V., Dieckmann, T., Butcher, S.E. and Feigon, J. (1996) *J. Biomol. NMR*, **7**, 83–87.
Sklenář, V., Dieckmann, T., Butcher, S.E. and Feigon, J. (1998) *J. Magn. Reson.*, **130**, 119–124.
Sörensen, O.W., Eich, G.W., Levitt, M.H., Bodenhausen, G. and Ernst, R.R. (1983) *Prog. NMR Spectrosc.*, **16**, 163–192.
Tate, S., Ono, A. and Kainosho, M. (1994) *J. Am. Chem. Soc.*, **116**, 5977–5978.
Tate, S., Ono, A. and Kainosho, M. (1995) *J. Magn. Reson.*, **B106**, 89–91.
Varani, G., Aboul-ela, F., Alain, F. and Gubster, C.C. (1995) *J. Biomol. NMR*, **5**, 315–320.
Weigelt, J. (1998) *J. Am. Chem. Soc.*, **120**, 10778–10779.
Wijmenga, S.S., Heus, H.A., Leeuw, H.A.E., Hope, H., van der Graaf, M. and Hilbers, C.W. (1995) *J. Biomol. NMR*, **5**, 82–86.
Wüthrich, K. (1986) *NMR of Proteins and Nucleic Acids*, Wiley, New York, NY.